

Crystal Engineering in Two Dimensions: An Approach to Molecular Nanopatterning

Krishna G. Nath,^{†,||} Oleksandr Ivashenko,[‡] Jennifer M. MacLeod,[†] Jill A. Miwa,[†]
James D. Wuest,[§] Antonio Nanci,[#] Dmitrii F. Perepichka,^{*,‡} and Federico Rosei^{*,†}

Centre Énergie, Matériaux et Télécommunications, Institut National de la Recherche Scientifique, 1650 Boulevard Lionel-Boulet, Varennes (QC), Canada J3X 1S2, Department of Chemistry, McGill University, 801 Sherbrooke St. West, Montréal, QC, Canada H3A 2K6, and Département de Chimie and Faculté de Médecine Dentaire, Université de Montréal, Montréal, QC, Canada H3C 3J7

Received: August 5, 2007

We describe a surprising cooperative adsorption process observed by scanning tunneling microscopy (STM) at the liquid–solid interface. The process involves the association of a threefold hydrogen-bonding unit, trimesic acid (TMA), with straight-chain aliphatic alcohols of varying length (from C₇ to C₃₀), which coadsorb on highly oriented pyrolytic graphite (HOPG) to form linear patterns. In certain cases, the known TMA “flower pattern” can coexist temporarily with the linear TMA–alcohol patterns, but it eventually disappears. Time-lapsed STM imaging shows that the evolution of the flower pattern is a classical ripening phenomenon. The periodicity of the linear TMA–alcohol patterns can be modulated by choosing alcohols with appropriate chain lengths, and the precise structure of the patterns depends on the parity of the carbon count in the alkyl chain. Interactions that lead to this odd–even effect are analyzed in detail. The molecular components of the patterns are achiral, yet their association by hydrogen bonding leads to the formation of enantiomeric domains on the surface. The interrelation of these domains and the observation of superperiodic structures (moiré patterns) are rationalized by considering interactions with the underlying graphite surface and within the two-dimensional crystal of the adsorbed molecules. Comparison of the observed two-dimensional structures with the three-dimensional crystal structures of TMA–alcohol complexes determined by X-ray crystallography helps reveal the mechanism of molecular association in these two-component systems.

Introduction

Suitably designed molecules can associate spontaneously, thereby forming a variety of supramolecular structures and phases by processes of self-assembly. These processes are profoundly important in nature, and the distinctive properties of molecular aggregates have played a key role in the creation and evolution of living systems. Mimicking such properties in artificial materials promises exciting new opportunities in many areas of science and technology.^{1,2} The concept of self-assembly has been successfully applied to the synthesis of numerous zero-dimensional systems (e.g., catenanes and rotaxanes³), one-dimensional structures (e.g., organic nanotubes⁴ and supramolecular polymers^{5,6}), and two-dimensional (2D) periodic structures. Monolayers of molecules on solid surfaces are the most studied 2D structures of this type. They are formed by a combination of strong adsorbate–surface interactions and relatively weak adsorbate–adsorbate interactions (e.g., thiols on gold^{7,8}) or by combinations in which adsorbate–adsorbate interactions are predominant (2D self-assembled molecular networks, or SAMNs). The latter have been studied intensively in the past decade, due to progress in scanning tunneling microscopy (STM), which allows imaging of SAMNs on conductive surfaces with sub-molecular resolution.^{9–19}

The basic principles and interactions that govern the formation of 2D-SAMNs also control the assembly of molecules in three-dimensional (3D) crystals. Molecular crystals have been studied for decades by X-ray crystallographic analysis, which provides exact atomic positions.^{20a} Although hundreds of thousands^{20b} of structures have been solved to date, our ability to predict and control molecular packing in crystalline materials is still limited. Achieving such control is the principal goal of the rapidly evolving field of crystal engineering,²¹ which has broad implications for many disciplines, including materials science²² and pharmaceutical science.²³

Combining the complementary methods and principles of 3D crystal engineering with those of 2D self-assembly will create unique opportunities for advances in science and technology. In particular, 3D crystallographic analysis offers the advantage of providing precise information about atomic positions, but the higher dimensionality of 3D crystals makes detailed evaluation of intermolecular interactions inherently more difficult. Moreover, X-ray crystallographic analyses are best suited to periodic structures that enjoy relatively high kinetic and thermodynamic stability. In contrast, 2D-SAMNs have fewer interactions per molecule, which simplifies their analysis. In addition, they can be investigated by STM, which allows direct-space imaging of structures that have multiple domains, structures that are aperiodic, and even structures that are in the process of being formed. In this paper, we present an example of a study that integrates 3D and 2D structural analysis, and we show how such studies can shed important new light on how molecular aggregation can be controlled rationally by combining hydrogen bonding and van der Waals interactions.

* Corresponding authors. E-mail: dmitrii.perepichka@mcgill.ca (D.F.P.); rosei@emt.inrs.ca (F.R.).

[†] Institut National de la Recherche Scientifique.

[‡] McGill University.

[§] Département de Chimie, Université de Montréal.

[#] Faculté de Médecine Dentaire, Université de Montréal.

^{||} Present address: Corning Technology Center, CORNING, 12117 Obuchi, Kakegawa, Shizuoka 437–1397, Japan.

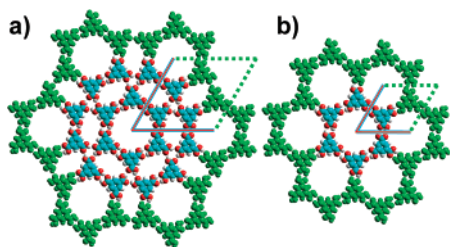


Figure 1. Molecular models of “flower” (a) and “chicken wire” (b) polymorphs of TMA-formed 2D-SAMNs on an HOPG interface (for the actual STM images see ref 15 and the Supporting Information).

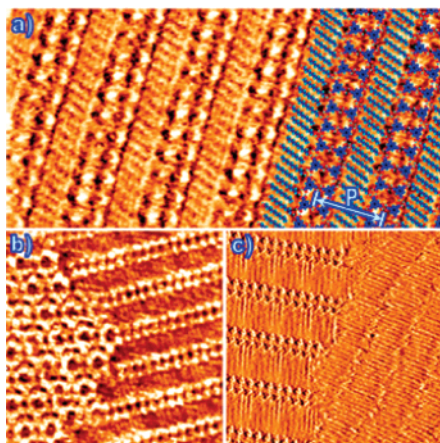
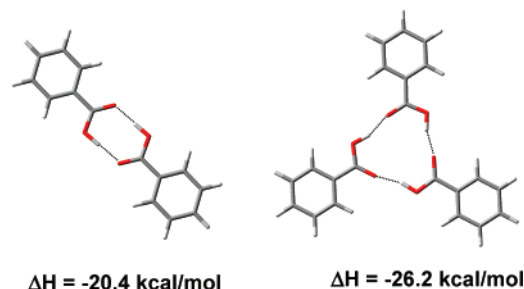


Figure 2. STM images of 2D-SAMNs produced by exposing HOPG to various solutions. (a) TMA/1-decanol in heptanoic acid. (b) TMA/1-undecanol in heptanoic acid. (c) TMA/1-heptacosanol (C_{27}) in octanoic acid. Image sizes: (a) $17.4 \times 8.7 \text{ nm}^2$, (b and c) $20.5 \times 20.5 \text{ nm}^2$. Tunneling parameters: (a) $V_s = -0.94 \text{ V}$, $I_t = 107 \text{ pA}$, (b) $V_s = -0.80 \text{ V}$, $I_t = 150 \text{ pA}$, and (c) $V_s = -0.80 \text{ V}$, $I_t = 300 \text{ pA}$.

In the majority of SAMNs studied previously, hydrogen bonding is the primary link among adjacent molecules, and it can be considered to govern the resulting structure. Among the most extensively studied SAMNs are those derived from 1,3,5-benzenetricarboxylic acid (trimesic acid = TMA), a molecule with potential C_3 symmetry. Because carboxyl groups ($-\text{COOH}$) tend to associate as cyclic hydrogen-bonded pairs, TMA is inherently disposed to form hydrogen-bonded sheets, both within crystals and on surfaces.^{14–16,24–26} The molecular C_3 symmetry of TMA is mirrored by the self-assembled hexagonal structures that result when TMA is adsorbed on suitable surfaces (graphite,^{14–16} Au,^{24,26} and Ag/Si(111)- $(\sqrt{3} \times \sqrt{3})R30^\circ$), both under vacuum and at the solution–solid interface. Furthermore, the trigonal symmetry of TMA should be reinforced by the underlying threefold symmetry of the substrate, thereby favoring hexagonal patterns and excluding different periodic motifs,²⁷ although other geometries have been observed in over- and underpotential conditions using electrochemical STM.²⁴

In a recent communication, we used STM imaging to reveal the creation of a new, unexpected pattern of self-association of TMA at the solution–graphite (highly oriented pyrolytic graphite, HOPG) interface, modulated by the coadsorption of alcohols.²⁸ We have also studied the formation of this pattern in the presence of fullerene, where the higher resolution that arises from adsorption of fullerene on the STM tip allowed us to detect a variety of quasi-stable self-assembled TMA structures while the system was approaching an equilibrium.²⁹ We now present a combined 3D and 2D study of the TMA–alcohol SAMNs, using both crystallography and STM imaging, and report detailed analyses of the adsorbate–surface and adsorbate–adsorbate interactions. Our studies cover such subtle phenomena

SCHEME 1: Calculated Gas-Phase Geometries and Hydrogen-Bonding Enthalpies for Benzoic Acid Dimer and Trimer at the B3LYP/6-31G(d,p) Level



as ripening and dynamics, the templating effect of the underlying graphite lattice, moiré patterns, expressions of chirality, and the effect of alcohol length and parity. The developed understanding of these effects allows us to alter the periodicity of 2D molecular nanopatterns in a rational way. The observed phenomenology is surprisingly rich, and it makes TMA–alcohol SAMNs a model for investigating the role of intermolecular interactions in other 2D-SAMNs and in 3D crystals.

Results and Discussion

Formation of Multicomponent Self-Assembled Molecular Networks. Two polymorphs have been observed when TMA is adsorbed on surfaces (Figure 1).^{16,30–32} Both structures have threefold symmetry, and all carboxyl groups participate fully in hydrogen bonding, either by normal dimeric pairing or by a hybrid combination of dimeric and trimeric association (Scheme 1). Griessl et al. observed these two structures³³ under UHV and named them the “chicken wire” and “flower” structures, respectively.¹⁶ Subsequent investigations at the solution–solid interface demonstrated that the chicken wire structure is formed preferentially when long-chain carboxylic acids are used as the solvent, whereas short-chain acids ($<C_7$) favor the flower structure.¹⁵ STM images of adsorption on HOPG from TMA/heptanoic acid solutions indicate that both chicken wire and flower structures are formed simultaneously. According to our density functional theory (DFT) calculations, hydrogen bonds in the cyclic dimer of benzoic acid, as present in the chicken wire network, are 1.5 kcal/mol stronger in the gas phase than those in the cyclic trimer, as present in the flower structure (Scheme 1). It is not clear to what extent the principle of closest packing³⁴ applies to 2D-SAMNs that form open structures in which significant parts of the underlying surface are left exposed to solvent; however, this principle suggests a possible preference for the more compact flower structure. The competition between intrinsically stronger intermolecular association (chicken wire structure) and tighter packing (flower structure) presumably determines which polymorph will be formed, and it explains the coexistence of both structures under certain conditions.

Although TMA freely adsorbs on HOPG from solutions in carboxylic acids, it has not been observed to adsorb from alcohol solutions. Instead, saturated solutions of TMA in 1-octanol, 1-decanol, and 1-undecanol gave only surface patterns due to the adsorbed alcohol (see the Supporting Information). This may be due in part to the low solubility of TMA in higher alcohols (e.g., $<0.01\%$ w/w at 20°C in 1-undecanol). Adding heptanoic acid to TMA/alcohol solutions resulted in the appearance of strikingly different linear patterns, which cannot be attributed to any of the components alone (Figure 2a). A detailed view of the observed linear patterns reveals tapes of dimerized molecules of TMA separated by intervening lamellas of alcohol, which

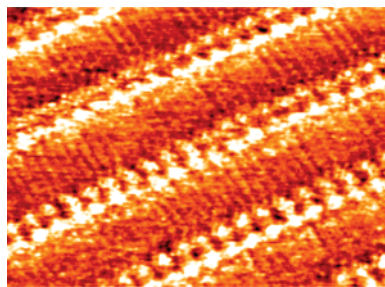


Figure 3. STM image of a TMA/1-heptadecanol SAMN on HOPG prepared by drop-casting from water suspension of the components. Image area: $18.0 \times 13.4 \text{ nm}^2$. Tunneling parameters: $V_s = -1.8 \text{ V}$, $I_t = 150 \text{ pA}$.

coadsorb on the substrate. Individual molecules are easily identified, establishing a 1:1 TMA–alcohol ratio in the SAMNs. Similar patterns were formed using alcohols of various lengths (see below), thereby allowing rational modulation of the periodicity of the pattern by varying the length of the alcohol component of the mixture. The new two-component TMA/alcohol patterns are thermodynamically more stable than those formed by either of the components individually. Domains formed by TMA alone or alcohol alone can be observed as transients, but eventually they are replaced irreversibly by the linear pattern characteristic of coassembly (Figure 2, parts b and c).

In this system, heptanoic acid was commonly used to help solubilize TMA. However, the same tape nanopatterns can easily be obtained with other solvents, including different fatty acids (propionic, hexanoic, octanoic and nonanoic) and 1,2,4-trichlorobenzene (see the Supporting Information). In addition, we also examined the formation of 2D-SAMNs in water, which may be of interest in applications related to biology. The use of water as a medium for self-assembly of TMA–alcohol SAMNs is not trivial because of the negligibly low solubility of higher alcohols in this solvent. Also, we found that the samples should be dried before imaging to avoid the high leakage current associated with STM imaging in water. Nevertheless, applying a dilute suspension of TMA and 1-heptadecanol in distilled deionized water has resulted in the formation of SAMNs identical to those observed in organic solvents (Figure 3). This shows that the TMA–alcohol SAMNs are formed as a stable motif under a wide variety of preparation conditions, which is important for their possible use as surface templates.

Nature of TMA–Alcohol Bonding in 2D-SAMNs. Hexagonal networks are the expected result of the self-association of threefold symmetric TMA,³⁵ so the consistent ability of alcohols to alter this preference is striking and requires explanation. Two possible hypotheses were examined to explain the formation of the observed SAMNs. In one hypothesis, covalent bonding between an alcohol and TMA occurs to form a monoester, which no longer has threefold symmetry. In the other hypothesis, the alcohol and TMA interact noncovalently via hydrogen bonding to form the observed linear patterns. Although the lengths of the covalent and hydrogen bonds implied by these two hypotheses are different, the resolution of STM is not high enough to let us measure these distances with sufficient accuracy to test these hypotheses.

The esterification of aromatic carboxylic acids is not expected to proceed readily at room temperature in the absence of catalysis by strong acids. However, only extremely small quantities are needed to form a monolayer if adsorption is preferential; moreover, 5-octadecylisophthalic acid, a molecule structurally related to the hypothetical monoester, was previously

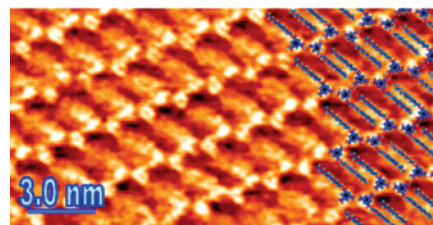
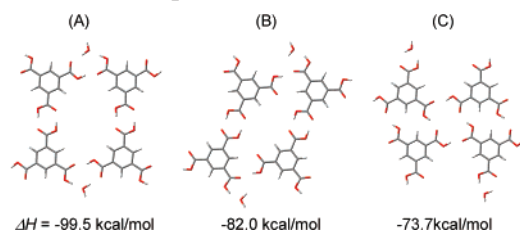


Figure 4. STM image of the SAMN formed from the 1-undecyl monoester of TMA on HOPG. The image shows a pattern distinctly different from that produced by exposing HOPG to mixtures of TMA/1-undecanol/heptanoic acid (Figure 2b). Tunneling parameters: $V_s = -1.7 \text{ V}$, $I_t = 100 \text{ pA}$.

observed to produce a similar SAMN.¹¹ Together, these factors made it essential to exclude the monoester hypothesis rigorously. After a mixture of TMA/1-undecanol/heptanoic acid in proportions similar to those used in the STM experiments was kept at $100 \text{ }^\circ\text{C}$ for 1 h, analysis by NMR spectroscopy and mass spectrometry provided no evidence for the presence of the 1-undecyl monoester of TMA, although a trace amount of 1-undecyl heptanoate was detected in the mass spectrum. We then prepared an authentic sample of the 1-undecyl monoester of TMA by the pyridine-catalyzed reaction of 1,3,5-benzenetricarbonyl trichloride with 1-undecanol. However, an STM image of the SAMN derived from the monoester (Figure 4) showed a pattern of self-assembly completely different from that of the tapes formed by TMA in the presence of alcohols. Instead, molecules of the monoester are linked via hydrogen-bonded pairs of carboxylic groups into zigzag arrays, which are held together in a 2D grid through van der Waals interactions of the alkyl chains. The lattice parameters for this monolayer are $1.65 \pm 0.05 \text{ nm}$ (along the TMA chain) and $3.33 \pm 0.05 \text{ nm}$ (along the axis of alkyl chains), which are very different from the corresponding unit cell parameters of 1-undecanol/TMA SAMNs (0.97 ± 0.05 and $3.36 \pm 0.03 \text{ nm}$, respectively). This observation allows us to unambiguously rule out the esterification hypothesis, thus leaving molecular association of TMA with alcohols via hydrogen bonding as the origin of the observed tapes.

Assembly of Hydrogen-Bonded TMA Tapes. The STM images of SAMNs formed by the coadsorption of TMA and alcohols on HOPG provide compelling evidence for the presence of tapes consisting of a double row of TMA molecules, presumably linked by hydrogen bonds. It is possible to imagine various orientations of the TMA molecules in these tapes that are consistent with both the trigonal geometry of TMA and the standard hydrogen-bonding motifs of carboxyl groups. In particular, the tapes can be considered to be constructed from tetrameric units with geometries **A**, **B**, and **C**, which correspond to rotations of 0° , $60^\circ/120^\circ$, and 180° of TMA with respect to the tape axis (Scheme 2). The geometries of these tetramers, bounded by two molecules of water (used instead of alcohols to confer planar D_{2h} symmetry to the models), were optimized using DFT with hybrid density functional (B3LYP/6-31G(d,p)). In these calculations, symmetry was constrained to be D_{2h} to model the unit cell of the tape. Three minima corresponding to aggregates **A**, **B**, and **C** were found, and the gas-phase enthalpy of association of the lowest-energy aggregate (**A**) is predicted to be 17.5 kcal/mol lower than that of the closest alternative (**B**).³⁶ The large preference for aggregate **A** suggests that it is likely to be favored in condensed phases as well. Indeed, a recent crystallographic study of the hydrogen-bonded 1:1 complex formed by TMA and methanol reports a closely related structure,³⁷ further supporting our conclusion that the observed tapes assemble according to motif **A**. Furthermore, the distances

SCHEME 2: Structures and Enthalpies of Association for Potential Hydrogen-Bonded Tape-Forming Aggregates A, B, and C of TMA, as Estimated by DFT Calculations at the B3LYP/6-31G(d,p) Level^a



^a The observed unit cell of the tapes is modeled by tetrameric aggregates of TMA bound by two molecules of water.

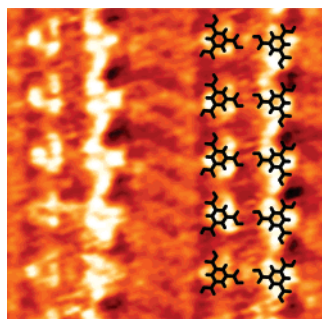


Figure 5. Submolecular detail of TMA tapes formed by coadsorption with 1-decanol. Image area: 5.3×5.3 nm². Tunneling parameters: $V_t = -0.68$ V, $I_t = 107$ pA.

between the centers of neighboring TMA molecules in the crystallographic study and in the calculated structure **A** are both ~ 0.96 nm, which agrees closely with the separation observed between the bright spots along the TMA tapes in Figure 2a (0.97 ± 0.05 nm).

Strong additional support for the presence of motif **A** was provided by high-resolution STM images, which revealed the internal structure of the tapes (Figure 5). TMA molecules in one tape are represented as equilateral triangles (sides equal to 0.40 ± 0.05 nm), with their bases oriented toward each other and separated by 0.70 ± 0.05 nm. These parameters closely match the positions of hydrogen atoms attached to the benzene rings of two molecules of TMA that engage in formation of a cyclic hydrogen-bonded dimer, as postulated in structure **A** (0.43 and 0.70 nm, respectively). The same submolecular resolution of TMA, with bright protrusions centered on these hydrogen atoms, has been described elsewhere in the literature for pure TMA SAMN.¹⁶

Structural Features of Alcohol Lamellas. The behavior of the alcoholic component of TMA–alcohol SAMNs is governed by three main factors: (1) interaction of the alkyl chains with the underlying HOPG surface, (2) intermolecular van der Waals interactions between the chains, and (3) hydrogen bonding of the OH groups with TMA. These three factors are analyzed in the following paragraphs.

Orientation of the Alkyl Chains. In principle, aliphatic hydrocarbon chains can adsorb on graphite in extended conformations with the zigzag plane being either parallel ($\Theta = 0^\circ$), orthogonal ($\Theta = 90^\circ$), or inclined ($0 < \Theta < 90^\circ$) with respect to the underlying surface (Figure 6). The parallel and orthogonal orientations are expected to be similar in energy, since they provide an equal number of C–H $\cdots\pi$ interactions with graphite (an average of one interaction per methylene unit). The inclined orientation, although closely related to the observed packing of alkanes in 3D crystals,³⁸ is expected to be disfavored

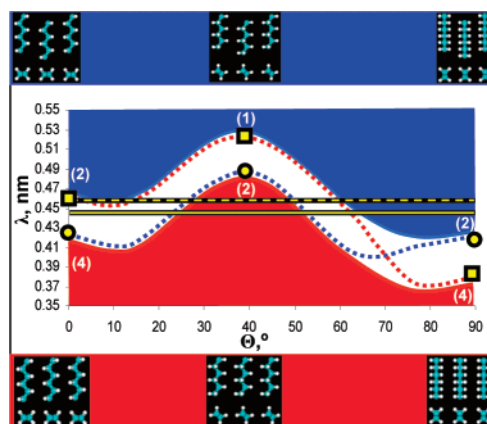


Figure 6. Possible arrangements (plane and cross section views) of close-packed aliphatic hydrocarbon chains on a surface in extended conformations, in both staggered and eclipsed mutual orientations. Θ is the inclination angle between the underlying surface and the zigzag plane of the chain, and λ is the interchain separation. The graph shows how the separation of chains, in both staggered (○) and eclipsed (□) orientations, will change with Θ when they are constrained to remain in van der Waals contact ($H\cdots H$ distance = 0.24 nm). The dashed curves correspond to rotation of the chains starting ($\Theta = 0^\circ$) from staggered (red) and eclipsed (blue) orientations. Such a rotation of the chains results in a transition between the staggered and eclipsed orientations at $\sim 70^\circ$. In parentheses are the numbers of van der Waals contacts per methylene unit between the chains in the specific orientation. The red and blue areas represent orientations with repulsive interactions ($H\cdots H$ distance < 0.24 nm) and weakened interactions ($H\cdots H$ distance > 0.24 nm), respectively. The white area defines where normal van der Waals contacts can be achieved by allowing the alkyl chains to shift slightly between the limiting staggered and eclipsed orientations. The yellow solid and broken lines show the experimental interchain separations for even and odd alcohols, respectively (see discussion of moiré pattern).

because it offers only half as many C–H $\cdots\pi$ interactions with graphite (but it cannot be completely ruled out since it would permit closer contacts between the chains).

The first two orientations should be readily distinguishable by high-resolution STM, which should reveal each methylene unit in the parallel orientation and a linear array of every second methylene unit in the orthogonal orientation (Figure 6). The inclined orientation is expected to appear as a linear array (of “high” hydrogens in every second methylene unit), and thus might be difficult to distinguish from the orthogonal orientation.³⁹

Many self-assembled monolayers formed on HOPG by compounds with long alkyl chains have previously been characterized by STM. Simple straight-chain alkanes^{10,40,41} adsorb in extended conformations that exhibit both parallel and orthogonal orientations with respect to the underlying surface, depending on the conditions. However, substituted derivatives typically favor only one of the two possibilities. We are not aware of any reports of compounds with extended alkyl chains that are adsorbed on graphite in intermediate (inclined) orientations. In high-resolution STM studies of the coadsorption of TMA and aliphatic alcohols containing an even number of carbon atoms, each methylene unit can be discerned, suggesting their parallel orientation on the surface (Figure 7a). In contrast, only every second methylene unit of the chains of odd alcohols was normally visible by STM (Figure 7b). In this case, the alkyl chains were observed as linear rows of dots separated by 0.25 nm, which agrees well with the expected 0.256 nm spacing between alternating methylene units in an extended aliphatic chain. This indicates a preferred orthogonal orientation (or inclined; see the Supporting Information) of odd alcohols on

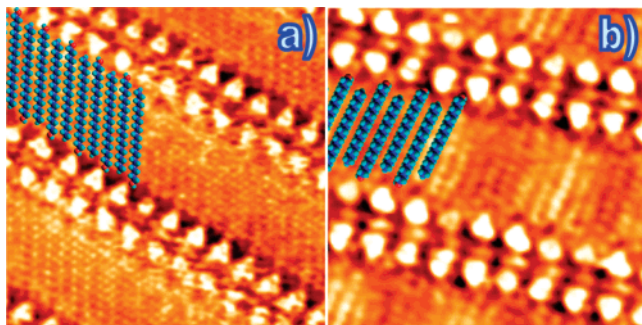


Figure 7. High-resolution STM images showing SAMNs derived from the coadsorption of TMA on HOPG with representative aliphatic alcohols containing odd or even numbers of carbon atoms. (a) 1-Docosanol (C_{22}) appears to lie parallel to the surface. (b) 1-Heptadecanol (C_{17}) appears to favor an extended conformation in which the zigzag plane is orthogonal or highly inclined with respect to the underlying surface. Image sizes: $10.8 \times 10.8 \text{ nm}^2$ (a) and $8.3 \times 8.3 \text{ nm}^2$ (b). Tunneling parameters: $V_s = -1.6 \text{ V}$, $I_t = 300 \text{ pA}$ (a) and $V_s = -0.88 \text{ V}$, $I_t = 90 \text{ pA}$ (b).

graphite, although substantial disorder was observed in such alcohol lamellas (see below).

In ideal tapes formed from TMA and an alcohol, the alkyl chains will pack closely to maximize their van der Waals interactions. For both parallel and orthogonal orientations of the chains on the underlying surface, a staggered orientation of adjacent chains provides for the largest number of van der Waals contacts (Figure 6). The best packing arrangements of staggered alkyl chains are characterized by interchain distances of 0.425 and 0.382 nm, in the parallel and orthogonal orientations, respectively. Both of these distances are shorter than the experimentally found interchain distances of $0.456 \pm 0.002 \text{ nm}$ (for odd alcohols) and $0.447 \pm 0.002 \text{ nm}$ (for even alcohols) (measured from the moiré pattern, see below). Comparison of these experimental values (represented by yellow lines in Figure 6) with the theoretical interchain distances (which depend on the inclination and the mutual shift of the alkyl chains) shows that a highly inclined orientation ($\Theta \sim 45^\circ$) is not possible (it would result in prohibitively close contacts, red area), the orthogonal orientation ($\Theta \sim 90^\circ$) is possible but would result in less-than-favorable interchain contacts ($>0.24 \text{ nm}$), and the parallel orientation ($\Theta \sim 0^\circ$) is the most favorable, with the optimum van der Waals interaction achieved somewhere between a completely staggered and completely eclipsed mutual orientations (between a circle and a square in Figure 6).

On the other hand, the actual interchain distances, particularly for even alcohols (see below), are shorter than half of the unit cell parameter along the TMA tapes (0.48 nm, two alcohols per unit cell). This mismatch is due to a tilt of the chains with respect to the TMA tapes. Analogous tilts are routinely observed in monolayers of functionalized alkanes (e.g., alkanethiols) assembled on metal surfaces; in these structures, tilting the alkyl chains away from the surface normal allows close packing, despite the inherent mismatch between the periodicities of the surface and the close-packed hydrocarbon chains.⁸ In TMA/alcohol SAMNs, a tilt of the alkyl chains with respect to the TMA tapes allows the chains to be in van der Waals contact at calculated tilt angles α of 62° (in the parallel orientation).

Our observations show that tilting of the alkyl chains is correlated with the parity of the number of carbon atoms in the chain. Typical tilt angles, as well as other physical parameters, are given in Table 1 for the nine alcohols studied. A pattern can be clearly discerned: alcohols with odd parity orient themselves nearly perpendicular to the TMA tapes,

TABLE 1: Geometric Features of SAMNs Formed by Coadsorbing TMA and Aliphatic Alcohols on HOPG

alcohol	$L \text{ (nm)}^a$	$P \text{ (nm)}^b$	$\alpha \text{ (deg)}^c$
$C_7H_{15}OH$	1.06	2.74 ± 0.16	83 ± 2
$C_8H_{17}OH$	1.19	2.69 ± 0.12	64 ± 2
$C_{10}H_{21}OH$	1.44	2.91 ± 0.07	64 ± 2
$C_{11}H_{23}OH$	1.57	3.36 ± 0.09	86 ± 2
$C_{16}H_{33}OH$	2.21	3.57 ± 0.10	66 ± 2
$C_{17}H_{35}OH$	2.34	4.10 ± 0.09	83 ± 2
$C_{22}H_{45}OH$	2.99	4.29 ± 0.07	64 ± 3
$C_{27}H_{55}OH$	3.63	5.32 ± 0.15	82 ± 3
$C_{30}H_{61}OH$	4.02	5.08 ± 0.11	66 ± 2

^a Calculated length of the alcohol in its fully extended conformation, as measured between the terminal hydrogens (DFT B3LYP/6-31G).

^b Period of the pattern (see Figure 2a). ^c Angle between the axis of the tapes and alkyl chains.

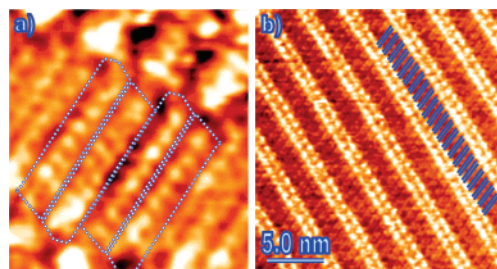


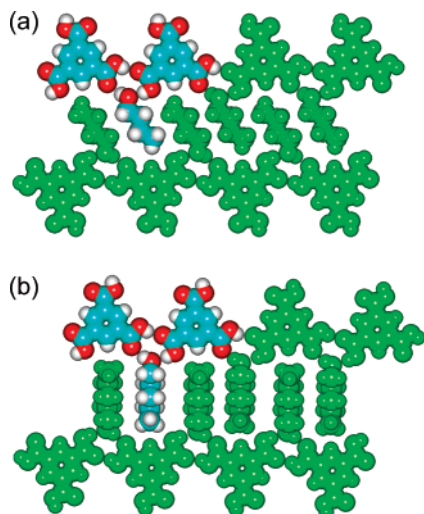
Figure 8. Manifestations of loose packing of the alkyl chains in TMA-alcohol SAMNs on HOPG. (a) Rotational disorder in a typical TMA/1-heptadecanol (C_{17}) SAMN; the blue lines delimit individual alcohol molecules. (b) Dimerization of alcohol chains in a TMA/1-hexadecanol (C_{16}) SAMN; the blue lines show individual alcohol molecules, arranged into tight pairs. Image size of (a) is $3.5 \times 3.9 \text{ nm}^2$. Tunneling parameters: (a) $V_s = -0.88 \text{ V}$, $I_t = 90 \text{ pA}$ and (b) $V_s = -1.4 \text{ V}$, $I_t = 90 \text{ pA}$.

whereas alcohols with even parity are tilted to values nearer to 65° . Due to relatively denser packing, such tilted structures (formed by even alcohols) do not normally show disorder of the type observed for untilted lamellas (formed by odd alcohols) (Figure 8a). Instead, a further ordering via dimerization of even alcohol chains into tight pairs is often observed (Figure 8b). This dimerization behavior is further confirmed by fast Fourier transform (FFT) analysis.

Parity (Odd-Even) Effect. The parity (odd-even) effect has long been known to affect the properties of alkane derivatives and their packing in the solid state. More recently, this effect has been observed in SAMNs by STM.⁴² In general, this effect arises from the different symmetry of odd and even homologues, but the consequences of this difference can emerge in various ways. To understand the nature of the parity effect in our SAMNs, we examined the molecular structure of the postulated assemblies in greater detail.

Scheme 3 shows models in which the alkyl chains have two distinct orientations with respect to the TMA tapes, as observed experimentally. These models are based on hydrogen-bonding geometries determined by X-ray crystallographic analysis and also reproduced by DFT calculations using water in place of alcohols (see above). Because the position of the OH group of the alcohol is fixed by directional $C-O\cdots H$ and $C=O\cdots H$ bonds, an in-plane orientation of the alkyl chains can only be achieved when the chain has an extended conformation and the $H-O-C-C$ torsion angle is either 180° (trans) or 120° (gauche).⁴³ In the trans conformation, the alkyl chains form an angle of $\sim 60^\circ$ relative to the TMA tapes, and their zigzag plane is oriented parallel to the HOPG surface. In contrast, the gauche conformation results in an angle of $\sim 90^\circ$ with respect to the TMA tape, and the chain's zigzag plane is nearly perpendicular

SCHEME 3: Molecular Models of SAMNs Produced by the Coadsorption of TMA and Aliphatic Alcohols on HOPG, Showing the Structure for (a) Alcohols with Even Numbers of Carbon Atoms (C_4) and (b) Odd Numbers (C_5)



to the surface. A similar behavior is observed in SAMNs formed on Au(111) by pure aliphatic alcohols, where *trans*, *gauche*, and mixed conformations give rise to three different orientations of the alkyl chains.⁴⁴

In either orientation, the alkyl chains strive to pack as closely as possible, thereby maximizing van der Waals interactions. For alcohols with an even number of carbon atoms, the preferred staggered mutual position of close-packed alkyl chains will give rise to van der Waals contacts between the aromatic hydrogen atoms of TMA and the terminal CH_3 group of the alkyl chain (Scheme 3a). This arrangement is not favorable when the number of carbons is odd because terminal CH_3 groups cannot be placed in contact with aromatic hydrogens of TMA in the staggered mutual position of alkyl chains. Consequently, odd alcohols prefer an alternative with a tilt of $\sim 90^\circ$ relative to the TMA tapes (Scheme 3b). Such an orientation should optimize van der Waals contacts and $\text{C-H}\cdots\text{O}$ hydrogen bonds of terminal CH_3 groups (which are located slightly above the TMA plane) with the aromatic proton and carboxyl oxygens of TMA. For even alcohols, however, this 90° arrangement would place terminal CH_3 groups in the TMA plane, possibly resulting in a degree of steric repulsion. In contrast to our early assumption,²⁷ a staggered mutual orientation of alkyl chains is not preferred in the 90° tilted structure. The closest $\text{H}\cdots\text{H}$ interchain distances that can be achieved at tilt angles down to 80° are 0.322 nm for close-packed chains in the fully staggered arrangement and 0.298 nm in the fully eclipsed arrangement. Thus, van der Waals interactions appear to be maximized in the eclipsed arrangement (Scheme 3b), although even then the packing of the alkyl chains remains very loose. This model agrees with the experimentally observed tilt angles, as well as with high-resolution STM images, which show even alcohols with staggered chains parallel to the surface and odd alcohols oriented orthogonally on the surface and experiencing a larger degree of disorder.

Length Effect. One of the most appealing features of SAMNs produced by codepositing TMA and aliphatic alcohols is the possibility of modulating the periodicity of the observed pattern simply by changing the length of the alcohols, which are readily available commercially. In the set of alcohols studied (see Table 1), the period of the pattern can be correlated with the number of carbon atoms in the alcohol and its parity. Regression analyses

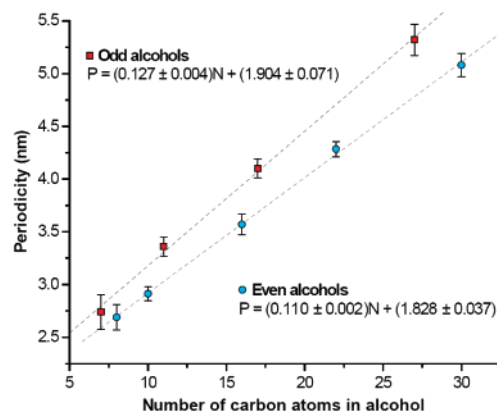


Figure 9. Periodicity in the TMA–alcohol SAMNs, showing the correlation with the number of carbon atoms in the alkyl chain of the alcohol.

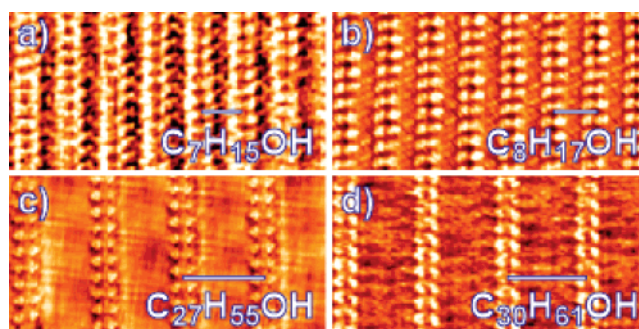


Figure 10. STM images of SAMNs of TMA with odd and even alcohols, showing those with the shortest periodicity (a and b) and the longest periodicity (c and d). The relative periodicity is indicated by scale bars above the formulas of the alcohols. Image size: $20 \times 10 \text{ nm}^2$ for all images. Tunneling parameters: $V_s = -0.55 \text{ V}$, $I_t = 305 \text{ pA}$ (a), $V_s = -0.87 \text{ V}$, $I_t = 250 \text{ pA}$ (b), $V_s = -0.80 \text{ V}$, $I_t = 300 \text{ pA}$ (c), $V_s = -2.04 \text{ V}$, $I_t = 214 \text{ pA}$ (d).

of the periodicity (P) in SAMNs formed with odd and even alcohols gave two different trends, from which tilt angles α of $82.3^\circ \pm 13.8^\circ$ and $59.2^\circ \pm 4.6^\circ$ could be extracted (Figure 9). The constant parameters in these regressions are 1.90 ± 0.07 and $1.83 \pm 0.04 \text{ nm}$ (for odd and even alcohols, respectively), which reflects the width of the TMA tape ($1.75 \pm 0.05 \text{ nm}$ measured from STM images) plus a small increment defined by hydrogen bonding between TMA and the alcohol.

In our studies, the periodicity of SAMNs was thereby modulated by a factor of ~ 2 , from 2.74 to 5.32 nm (Figure 10). In principle, structures with even greater periodicity can be attained by increasing the length of the alcohol, although a competitive formation of pure alcohol patterns will eventually prevail. Furthermore, the rate of formation of such SAMNs will be decreased by the slow dynamics of longer alcohols. This can be expected to affect the size of ordered domains, as well as the structure within the domains. For example, unexpectedly low alkyl tilts ($\alpha \geq 75^\circ$) were occasionally observed for 1-heptadecanol (C_{17}), and an anomalously high tilt ($\alpha \leq 74^\circ$) was observed for 1-triacontanol (C_{30}) near a domain boundary. On the other hand, the lower adsorption energies of short alcohols reduce the stability of the SAMNs. As a result, we could not observe the formation of SAMNs on HOPG with alcohols shorter than 1-heptanol. This length-specific behavior of SAMNs derived from TMA and aliphatic alcohols presumably contributed to the relatively high uncertainties that we observed in averaged periodicities for the shortest and the longest alcohols studied, as well as to the largest tilt angle distributions obtained from the regression analyses.

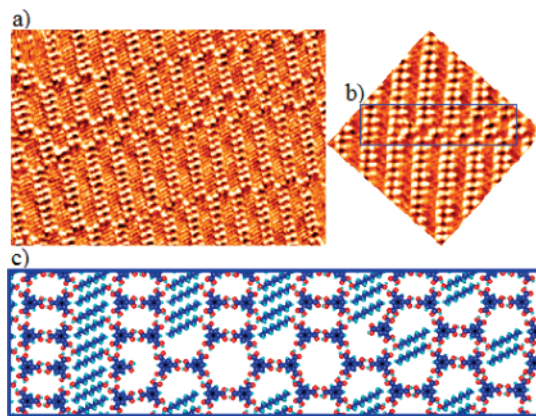


Figure 11. STM images of the TMA–octanol SAMN on HOPG, showing intermingling of TMA tapes with alcohol lamellas. (a) Large-area image showing multiple registry shifts in the TMA tapes. Image size: $37.2 \times 25.5 \text{ nm}^2$; $V_s = -0.85 \text{ V}$, $I_t = 80 \text{ pA}$. (b) Detailed image showing the initiation and development of the shift within a domain. Image size: $15.5 \times 15.5 \text{ nm}^2$; $V_s = -0.92 \text{ V}$, $I_t = 100 \text{ pA}$. (c) Molecular model of the highlighted area in (b).

Of special interest is the TMA/1-octanol system, which illustrates the richness of the architectures achievable in multicomponent SAMNs. In addition, this system highlights the unique power of real-space techniques such as STM for imaging structures that are locally ordered yet aperiodic, which is not possible with conventional reciprocal-space methods such as X-ray crystallography. In this system, a new structural motif appears as an occasional registry shift, where the TMA tape and alcohol lamella trade places (Figure 11). Such a shift requires a very close match between the widths of the TMA tape and the alcohol lamella, which can only be achieved with 1-octanol. Detailed analysis of the molecular arrangement shows that the shift is accomplished by a mirror-plane translation of TMA molecules in the tapes, giving a hybrid network with structural features similar to those of the classic hexagonal “chicken wire” TMA pattern (Figure 11c). Similar transitions between hexagonal arrangements of TMA and linear TMA–alcohol SAMNs have also been observed for other alcohols, albeit only at interfaces between domains. The formation of these deviant structures supports the proposed molecular orientation within the TMA tapes, as shown in Scheme 2. Among the three possible TMA tetramers, only structure **A** would allow bonding with “misplaced” TMA molecules at the observed 120° angle.

Chirality. Chirality is a well-known phenomenon in 3D space, observed in many naturally occurring molecular and supramolecular structures. Its manifestation in 2D space (i.e., on surfaces) is beginning to be explored, primarily by STM. Prominent examples include the determination of the absolute configuration of alkenes chemisorbed on the silicon (100) surface,⁴⁵ enantioselectivity in heterogeneous catalytic systems induced by the adsorption of chiral molecules,⁴⁶ and chiral specificity in the dimerization of cysteine adsorbed on Au.⁴⁷ Due to their particular hydrogen-bonded structures, the dimerized TMA tapes shown in Scheme 2 are prochiral. Their adsorption on a surface eliminates the symmetry element of reflection plane (σ) and forms enantiomeric structures. Although the resolution achieved by STM is not sufficient to clearly identify the two enantiomers of the TMA tapes themselves, they give rise to different tilts of the alkyl chains relative to the TMA tapes. This feature is readily observed in STM images.

In general, three possible scenarios⁴⁸ can describe 2D assemblies of chiral structures: (i) formation of racemic

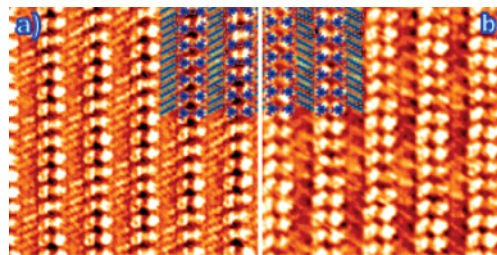


Figure 12. Manifestations of chirality in TMA–alcohol SAMNs on HOPG. STM images showing R (a) and L (b) domains in SAMNs prepared from TMA and 1-octanol. Image size: $13.5 \times 13.5 \text{ nm}^2$ (a and b). Image parameters: $V_s = -0.87 \text{ V}$, $I_t = 250 \text{ pA}$ (a) and $V_s = -0.93 \text{ V}$, $I_t = 278 \text{ pA}$ (b).

domains, in which the unit cell contains both enantiomers in a 1:1 “cocrystal”, (ii) formation of pseudoracemic domains, consisting of a mixture of randomly oriented enantiomers, or (iii) formation of chiral domains. The TMA–alcohol SAMNs proved to belong to the third group. Within each domain, only one of the two enantiomeric arrangements can be found (Figure 12, parts a and b). Alkyl chains on both sides of the TMA tapes are parallel and can be tilted either right (R-enantiomer) or left (L-enantiomer). Within a single domain, all alkyl chains are aligned in the same direction, whereas the orientation of lamella in different domains may vary (see the section “Interaction of the SAMNs with the Underlying HOPG Surface”).

Structures of 3D Cocrystals of TMA and Aliphatic Alcohols. X-ray crystallographic analysis can determine precise atomic positions in 3D crystals. This information complements data obtained by using STM to analyze the structure of 2D crystals on surfaces. Because of the spatial constraints and the templating effect of the surface, molecular packing in monolayers can be very different from what is observed in bulk crystals. Nevertheless, for some compounds supramolecular architectures of 2D and 3D crystals are similar (as is the case for TMA alone), in which case the precise atomic coordinates obtained from X-ray analysis are indispensable for a deeper understanding of the intermolecular interactions. The previous efforts in this direction include investigations of other hydrogen-bonding SAMNs,^{49a} macrocycles,^{49b,c} and oligothiophenes.^{49d} A particularly relevant example is the study of 5-hexadecyloxyisophthalic acid. When alone, it shows completely different packing in 2D and 3D crystals, but a very similar hydrogen-bonding pattern was found in 2D and 3D crystals of its complexes with pyrazine.^{49a}

However, such studies are limited since obtaining a single compound as both 2D and 3D crystals, suitable for dual studies using STM and X-ray crystallography, is a significant challenge, particularly when the crystals have complex compositions involving more than one component. More than 200 hydrogen-bonded aggregates of TMA and its anions with various hydrogen-bonding donors and acceptors have been studied by X-ray crystallography to date,^{21b} but only one crystal structure of a TMA–alcohol complex (with methanol) has been reported. To better understand the structural features of the observed 2D-SAMNs, as well as to probe the similarities between 2D and 3D assemblies, we grew single crystals of adducts of TMA with higher alcohols of varying length and parity. Samples suitable for analysis by X-ray diffraction were obtained by slow recrystallization of TMA from 1-butanol, 1-pentanol, and 1-hexanol.

TMA was found to cocrystallize with all three alcohols (as well as with methanol, as previously reported) to form tape structures that closely resemble those predicted by DFT calcula-

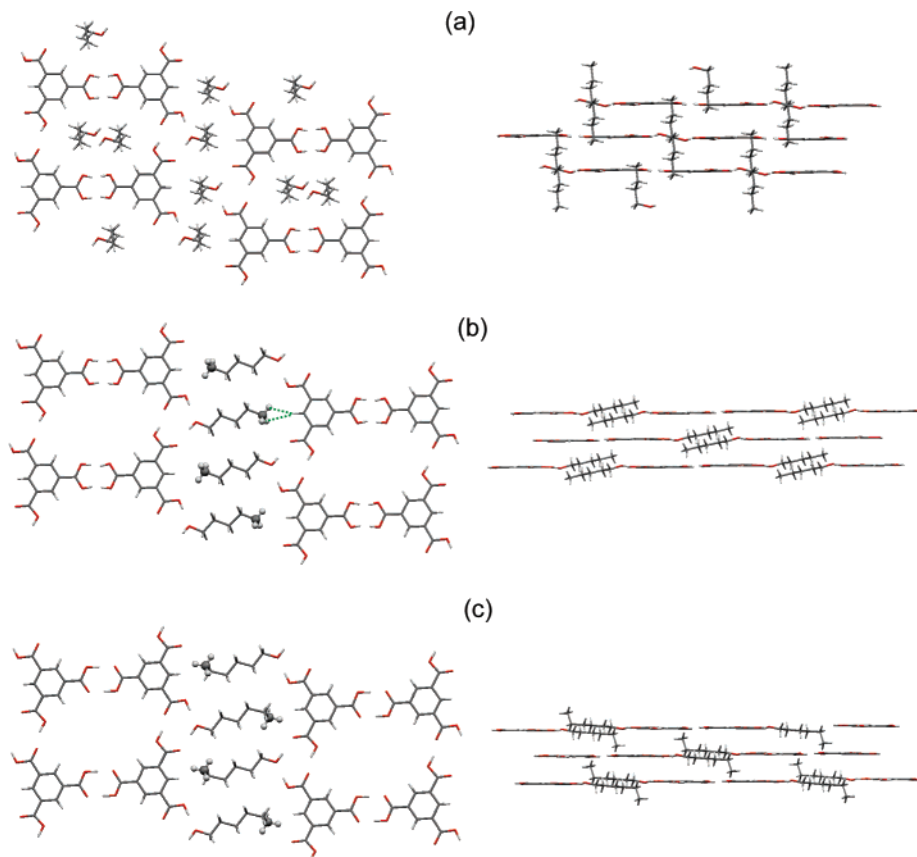


Figure 13. Views of the structures of 1:1 cocrystals of TMA with (a) 1-butanol, (b) 1-pentanol, and (c) 1-hexanol, showing the arrangement of molecules in sheets (left column) and the intersheet packing (right column).

tions and found by STM in 2D assemblies of TMA and aliphatic alcohols on HOPG (Figure 13). As in the 2D-SAMNs, the TMA tapes in 3D crystals are parallel and nearly coplanar. The mean planes of adjacent TMA tapes are displaced only by 0.009 nm in TMA/1-butanol, 0.004 nm in TMA/1-pentanol, and 0.038 nm in TMA/1-hexanol. This packing defines sheets, which are spaced by 0.345 nm in TMA/1-butanol, 0.315 nm in TMA/1-pentanol, and 0.325 nm in TMA/1-hexanol. This remarkable preservation of the self-assembly motif in 2D and 3D crystals, for alcohols ranging from CH_3OH to $\text{C}_{30}\text{H}_{61}\text{OH}$, clearly indicates its inherent stability.

The largest differences between the 2D and 3D structures proved to lie in the orientation of the alkyl chains. The underlying HOPG surface helps constrain adsorbed molecules in the 2D-SAMNs to lie in a plane, but there is no such constraint in 3D crystals. This fact, together with unoccupied space within the TMA tetramers, allows the alkyl chains to deviate from the plane of the sheet and to partially or fully occupy space within the tapes in adjacent sheets (Figure 13). The shortest alcohol studied, 1-butanol, cocrystallizes with TMA to form a structure in which the alkyl chains are nearly perpendicular to the TMA sheets and penetrate the cavities formed by TMA tetramers in the two adjacent sheets. Such an orientation is possible for 1-butanol, whose length (~ 0.4 nm for the extended $\text{OCH}_2\text{CH}_2\text{CH}_2\text{CH}_3$ chain, plus 0.24 nm for twice the van der Waals radius of hydrogen) matches the double intersheet spacing. In longer alcohols, however, this arrangement would lead to repulsion between the alkyl chains of every other sheet. Consequently, 1-pentyl and 1-hexyl chains adopt only a slight out-of-plane angle ($\sim 12^\circ$ and $\sim 5^\circ$, respectively) with respect to the TMA sheet. Both alcohols have the same trans $\text{H}-\text{O}-\text{C}-\text{C}$ conformation involving the hydroxyl group, and the alkyl chains are thereby tilted relative to the direction of

the TMA tapes by similar angles (75° and 71° for 1-pentanol and 1-hexanol, respectively). The slight difference is due to somewhat different out-of-plane angles for these alcohols. The similarity of the observed tilts in 3D crystals is in contrast to what we observed in 2D-SAMNs by STM, where distinctly different tilt angles were found for odd and even alcohols ($\sim 85^\circ$ and $\sim 65^\circ$, respectively). Apparently, an additional degree of freedom in 3D crystals (out-of-plane conformations) results in a different manifestation of the odd–even effect. For the odd alcohol (1-pentanol), the closest interactions between adjacent sheets are $\text{CH}_3 \cdots \text{CH}(\text{aromatic})$ contacts (Figure 13b, dotted lines). The aromatic hydrogen is situated between the hydrogens of two methyl groups, 0.27 nm away. The extra methylene group in even alcohols would bring this terminal CH_3 group into unacceptably close contact with the aromatic hydrogen. On the other hand, removing this repulsion by shifting chains relative to one another by two methylene groups (necessary to maintain the preferred staggered conformation) would leave volume unoccupied. As a result, repulsion is avoided by rotating the terminal CH_3 group out of the plain of the alcohol lamella to create a gauche $\text{C}-\text{C}-\text{C}-\text{C}$ conformation at the terminus of the chain. In the corresponding 2D-SAMNs, this would result in a loss of enthalpy of adsorption, so a change in the tilt angle occurs instead, accompanied by rotation of the $\text{H}-\text{O}-\text{C}-\text{C}$ torsion angle to assume a gauche conformation.

Interaction of the SAMNs with the Underlying HOPG Surface. The preceding analysis of 2D-SAMNs constructed from TMA and aliphatic alcohols has focused on intermolecular interactions, without considering the $\pi \cdots \pi$ and $\text{C}-\text{H} \cdots \pi$ interactions that help control adsorption of molecules on the surface of HOPG. Generally, binding is preferential for particular sites on the surface. Simple molecular mechanics calculations show two minima for the orientation of a linear alkane on a

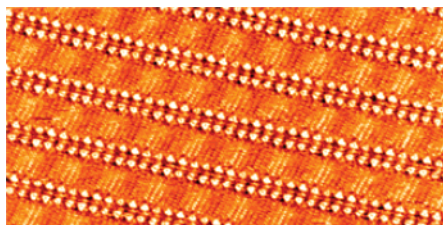


Figure 14. STM image showing moiré fringes in the alcohol lamellas of a SAMN coassembled from TMA and 1-heptadecanol (C_{17}). Image size: $34 \times 18 \text{ nm}^2$. Tunneling parameters: $V_s = -1.06 \text{ V}$, $I_t = 224 \text{ pA}$.

sheet of graphene: (1) a lower energy orientation along the zigzag direction of the sheet $[01\bar{2}0]$, with the maximum number of $C-H \cdots \pi$ interactions, and (2) a higher energy orientation along the “armchair” direction $[0010]$ (see the Supporting Information). The preferential adsorption of linear alkyl chains along the zigzag $[01\bar{2}0]$ direction of HOPG has been demonstrated for a variety of functionalized derivatives.⁵⁰ Our STM experiments revealed a similar preference. Abrupt change of the bias voltage during the acquisition of data provided an atomically resolved image of the HOPG substrate in the same frame as the TMA/alcohol SAMN. This image confirmed that the alcohols are oriented along the zigzag direction, as expected (see the Supporting Information).

Further manifestations of interactions between the SAMNs and HOPG are the superperiodic moiré patterns (MP) that arise from the mismatch of the periodicities of the alcohol lamellas and the underlying graphite surface.¹⁰ Figure 14 shows a representative STM image of a SAMN coassembled from TMA and 1-heptadecanol (C_{17}). Clear periodic contrast modulations can be seen within the alcohol lamellas. The number of alkyl chains per MP fringe can be used to obtain exact interchain distances with very high precision.^{50c} Thus, the interchain distances for TMA/alcohol SAMNs were $0.458 \pm 0.002 \text{ nm}$ for odd alcohols (6–7 alcohols per fringe) and $0.448 \pm 0.001 \text{ nm}$ for even alcohols (9.5–10 alcohols per fringe). Accounting for the tilt angle of the alcohols, which are determined directly from the images and suffer from larger errors, periodicities along the TMA tape of 0.92 ± 0.01 and 0.98 ± 0.01 were found for the odd and even alcohols, respectively. Both values are within the error bars of the periodicity obtained directly from the STM images ($0.97 \pm 0.05 \text{ nm}$). However, the difference between them suggests that the hydrogen-bonding association between TMA molecules is more flexible in 2D-SAMNs on HOPG than in 3D crystals (the relevant difference is 1 order of magnitude lower: 0.955–0.961 nm).

Domain Boundaries. Large-scale STM images of TMA–alcohol SAMNs often reveal multiple domains, with sizes ranging from tens to hundreds of nanometers (the maximum scan size providing molecular resolution). Capturing several domains within the same STM image shows that the mutual orientation of the TMA tapes in adjacent domains is not random. By analogy with 3D bicrystallography,⁵¹ the observed multidomain SAMNs can be classified as heterogeneous 2D bicrystals (consisting of ordered domains with different compositions and/or different structures, as in Figure 2, parts b and c) or as homogeneous 2D bicrystals (consisting of ordered domains with the same composition and structure but with different orientations, as in Figure 15). The homogeneous 2D bicrystals we have observed can be further subdivided into oriented bicrystals (Figure 15a), reflectional twins (Figure 15b), and rotational twins (Figure 15c). Nonoriented 2D bicrystals with no specific relationship between their component domains are also possible,

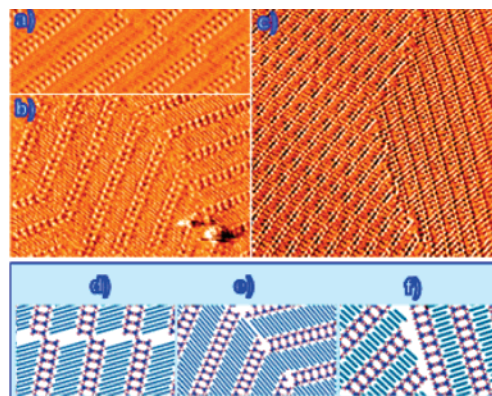


Figure 15. STM images of multidomain areas. (a and b) SAMNs prepared by depositing solutions of TMA and 1-docosanol (C_{22}) in octanoic acid. (c) SAMN prepared from a solution of TMA and 1-undecanol in heptanoic acid. (d–f) Molecular models of the domain boundaries shown in images (a–c), respectively. Image sizes: (a) $28.3 \times 10.3 \text{ nm}^2$, (b) $32.4 \times 21.9 \text{ nm}^2$, and (c) $56.3 \times 56.3 \text{ nm}^2$. Tunneling parameters: (a) $V_s = -1.20 \text{ V}$, $I_t = 300 \text{ pA}$, (b) $V_s = -0.80 \text{ V}$, $I_t = 300 \text{ pA}$, and (c) $V_s = -0.95 \text{ V}$, $I_t = 200 \text{ pA}$.

in principle, but were not observed due to the orientational effect of the underlying HOPG surface.

The mutual orientation of the domains is guided predominantly by attractive $C-H \cdots \pi$ interactions between the alkyl chains and HOPG, and the alcohols strongly prefer to be oriented along the main axes of HOPG (see the previous section). Although at domain boundaries, intermolecular interactions (van der Waals interactions between alcohols and hydrogen bonds) can make a particularly large contribution to the overall energy of interaction, their effect on the orientation of domains is likely to be felt only for very small domains.

In oriented bicrystals (Figures 15a), the alcohols are aligned along the same zigzag direction of HOPG, and the TMA tapes are shifted relative to one another, so that the two parts of interrupted tapes are linked by dimeric hydrogen-bonded association of carboxyl groups (Figure 15d). This behavior is very similar to the unique stacking fault observed for SAMNs composed of TMA and 1-octanol (see Figure 11 and related discussion). We note that this shift at domain boundaries does not create a mirror plane, and the chirality of adjacent domains is thereby preserved. Their basis vectors are oriented with respect to the same coordinate system,^{51a} and the TMA tapes in adjacent domains run in the same direction.

The alcohols in reflectionally twinned domains (Figure 15b) are also oriented along the same direction of HOPG; however, the associated TMA tapes are related by mirror-plane symmetry at the boundary (reflectional binary twin operation^{51b}), which inverts the chirality of the domain. The angle between the directions of TMA tapes is equal to the sum of the alcohol tilt angles (2α)⁵² of the adjacent domains (e.g., $\sim 2 \times 65 = 130^\circ$ for even alcohols).

In rotational twins (Figure 15c), the alkyl chains are oriented along different zigzag directions of HOPG, which are related by a 60° rotation because of the threefold symmetry of HOPG. Consequently, TMA tapes in adjacent domains intersect at 60° , and chirality is preserved. The intermolecular interactions at the boundaries of rotational twins are less favorable than those at the boundaries of co-oriented and reflectional twins, because alkyl chains in rotational twins are not parallel, and the TMA tapes are not commensurable. In theory, co-oriented twins are expected to be the most stable, followed by reflectional twins, and then by rotational twins. In practice, however, we observed co-oriented twins much less frequently than the two other forms.

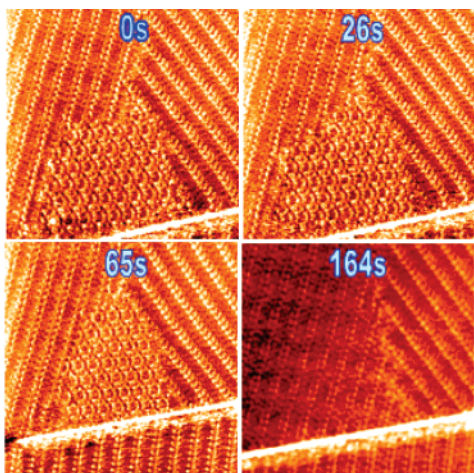


Figure 16. Time-lapse STM images showing the growth of the tapes of TMA/1-undecanol SAMNs at the expense of the flower structure consisting of pure TMA. Image size $36.25 \times 36.25 \text{ nm}^2$. Tunneling parameters: $V_s = -0.70 \text{ V}$, $I_t = 80 \text{ pA}$.

This can be rationalized by the likelihood that co-oriented twins are kinetically unstable: the high structural commensurability of the co-oriented domains requires only small molecular translations to produce a single domain, which reduces the activation barrier for ripening relative to those of less commensurable reflectional and rotational domains.

Dynamics and Stability of the TMA–Alcohol SAMNs.

Working at the solution/solid interface allows real-time observation of the assembly and evolution of SAMNs. In multicomponent systems, time-resolved imaging can elucidate the relative stability of different phases. In our system, the 2D flower pattern of pure TMA is thermodynamically less stable than the two-component tapes composed of TMA and alcohols, and the flower pattern is gradually replaced by the tapes as the system equilibrates (Figure 2b). Figure 16 shows time-lapse images that document the disappearance of TMA flower domains (see also the Supporting Information).

We believe that the TMA–alcohol tapes are more stable than structures composed of pure TMA or pure alcohol because of the interplay of two factors: (i) the adsorption enthalpy of individual molecules and (ii) intermolecular interactions in the formed monolayer. Although a pure TMA network has stronger intermolecular interactions, compared to networks of alcohols, the adsorption enthalpy of individual TMA molecules is not as high as that of larger alcohol molecules. The TMA–alcohol SAMNs enjoy both high adsorption enthalpy provided by alcohol chains and strong intermolecular interactions within the hydrogen-bonded network, making them thermodynamically more stable.

The effect of the higher adsorption enthalpy of larger molecules⁵³ can be observed in SAMNs formed from solutions containing two different aliphatic alcohols. Competition experiments performed using solutions containing TMA and equimolar amounts of 1-octanol and 1-heptadecanol showed that the surface was dominated by tapes containing the longer alcohol, given sufficient time for equilibrium to be established. However, the SAMNs formed immediately after deposition of the mixture contained only TMA and 1-octanol. A similar behavior has been recently reported for adsorption of a mixture consisting of the bis(1-heptadecyl) ester of isophthalic acid contaminated with a small amount of bis(1-heptadecyl) isophthalic anhydride.⁵⁴ In this case, a monolayer composed of the smaller diester formed initially but was eventually replaced by a more stable monolayer consisting of the larger anhydride. Similar kinetic effects

presumably underlie our observation of the initial dominance of SAMNs containing TMA and short-chain alcohols. Such structures can form more quickly, but domains containing lamellas of longer alcohols are more thermodynamically stable and eventually prevail.

Additional dynamic effects can be observed within SAMNs constructed from TMA and aliphatic alcohols. For example, it appears that formation of the hydrogen-bonded TMA tapes may be faster than the process by which the alcohols undergo 2D crystallization to produce close-packed lamellas. Tilt angles different from the characteristic final values (65° and 85° for even and odd alcohols, respectively) have been observed at the early stages of self-assembly, particularly for SAMNs built from longer alcohols. The evolution of multidomain regions provides additional information about the stability of SAMNs composed of TMA and alcohols. Over time (on the order of minutes), large-area domains are observed to consume bordering smaller domains, a behavior which is consistent with Ostwald ripening.

Conclusions

We have demonstrated that multicomponent SAMNs can be used in a rational way to create specific new 2D nanopatterns on atomically flat surfaces. The SAMNs studied in this paper, composed of TMA and aliphatic alcohols, are characterized by an unexpected linear nanopattern, despite the threefold symmetry of both TMA and the HOPG surface used as substrate. The structure of the SAMNs is defined by a complex combination of intermolecular van der Waals interactions and hydrogen bonds, as well as by site-specific molecule–surface interactions. The system is surprisingly rich, and it reveals an odd–even effect of the alkyl chain of the alcohol, an effect of length, the role of chirality, moiré patterns, and other noteworthy phenomena. By combining the principles of 2D self-assembly and 3D crystal engineering, we have gained a detailed understanding of the mechanisms responsible for the growth of these SAMNs. This understanding allows us to form the nanopatterns in a predictable way. Specifically, the periodicity of SAMNs constructed from TMA and alcohols can be modulated rationally by taking into account the length and parity of the alcohol component. The large domain size of the resulting 2D pattern, in which the periodicity of alternating hydrophobic/hydrophilic regions can be rationally modulated, suggests its possible exploitation as a nanoscale template. We expect that the relationships revealed in our work will be broadly applicable to other multicomponent molecular systems and will help engineer other SAMN-based nanopatterns, both in 2D and 3D.

Experimental Section

STM images were acquired from the current channel (inverted contrast) of a Digital Instruments Inc. (Veeco) NanoScope IIIa, as well as from the topography channel of a NanoSurf EasyScan2. Tips were mechanically formed from 80/20 or 30/70 PtIr wire (Goodfellow Corporation). The substrate graphite (SPI-2) was obtained from SPI Supplies. Calibration of the piezoelectric positioner was verified by atomically resolved imaging of graphite. TMA/alcohol solutions were prepared by dissolving ≈ 20 – 200 mg of alcohol in 1 mL of solvent, to which a sufficient amount of TMA (≈ 1 – 2 mg) to saturate the solution was added. Solutions were introduced between the tip and surface in $\sim 5 \mu\text{L}$ drops via syringe. All images presented in this paper have been Gaussian-smoothed using WSxM.⁵⁵

Density functional theory calculations were performed with the Gaussian W03 program.⁵⁶ Geometry was optimized at the B3LYP/6-31G(d,p) level. Planar symmetry constraints were

imposed in calculations of the TMA dimer and trimer (Scheme 1) and the $(\text{TMA})_4(\text{H}_2\text{O})_2$ aggregate (Scheme 2). The enthalpy of hydrogen-bonding association was calculated by subtracting the sum of total energies of all individual constituents (calculated at the same level) from the total energy of the complex.

Figure 6 was compiled from trigonometric calculations on molecular models placed with appropriate inclination angles and relative orientations (staggered and eclipsed) in close contact. The molecular parameters used in these calculations were the interatomic distances in an all-trans hydrocarbon chain (0.176 nm between geminal hydrogens, 0.251 nm between vicinal hydrogens) and the van der Waals radius of hydrogen (0.120 nm). The calculation gave values for interchain distances, as well as the number of close van der Waals interactions per methylene unit.

1-Hexanol (98%), 1-heptanol (98%), 1-octanol (99%), 1-decanol (99%), 1-undecanol (99%), 1-hexadecanol (95%), 1-heptadecanol (98%), 1-docosanol (98%), 1-heptacosanol (99%), 1-triacontanol (96%), 1,3,5-benzenetricarboxylic acid (95%), propionic acid (99.5%), hexanoic acid (99%), heptanoic acid (99%), octanoic acid (98%), nonanoic acid (98%), 1,2,4-trichlorobenzene (99+%), tridecane (99%), 1,3,5-benzenetricarbonyl trichloride (98%), anhydrous acetonitrile (99.8%), and pyridine (99%) were purchased from Sigma-Aldrich and were used without further purification.

1-Undecyl Monoester of TMA. To a stirred solution of 1,3,5-benzenetricarbonyl trichloride (3.09 g, 11.6 mmol) in anhydrous acetonitrile (5 mL) at 0 °C under N_2 was slowly added a solution of pyridine (0.92 g, 11.6 mmol) in acetonitrile (5 mL). The mixture turned purple, and a white precipitate was formed. After 20 min at 25 °C, a solution of 1-undecanol (1.00 g, 5.80 mmol) in acetonitrile (15 mL) was added dropwise. The white precipitate dissolved, and the resulting mixture was stirred at 25 °C for 7 h. More pyridine (1.84 g, 23.3 mmol) was added in one portion, resulting in the formation of a pink precipitate. After 30 min, the mixture was diluted with water (3 mL), and stirring was continued for another 2 h. The resulting white precipitate was filtered, washed with water (20 mL), and dissolved in diethyl ether (15 mL). The solution was washed with 1% aqueous HCl (15 mL) and then with water (2×20 mL). Solvent was removed from the organic layer by evaporation, leaving the crude product (0.450 g, 21.3% based on the alcohol) as a colorless solid that contained ~7% of TMA (according to ^1H NMR spectroscopy). Four recrystallizations from 0.5 M aqueous pyridine (ca. 10 mL) followed by neutralization with 1% HCl gave 0.075 g of analytically pure sample (>99%): ^1H NMR (300 MHz, $\text{DMSO}-d_6$) δ 13.58 (s, 2H), 8.61 (t, 1H, $J = 1.5$ Hz), 8.59 (d, 2H, $J = 1.5$ Hz), 4.30 (t, 2H, $J = 6.6$ Hz), 1.71 (m, 2H), 1.39–0.97 (m, 16H), 0.81 (t, 3H, $J = 6.9$ Hz); ^{13}C NMR ($\text{DMSO}-d_6$) δ 166.3, 164.9, 134.5, 133.9, 132.7, 131.5, 66.2, 32.1, 29.79, 29.77, 29.72, 29.54, 29.42, 28.8, 26.2, 22.9, 14.8; MS (ESI $^-$, %): 727 (100%, $[\text{M} - \text{H}]^-$), 363 (74%, $[\text{M} - \text{H}]^-$).

Acknowledgment. K.G.N. and O.I. contributed equally to this work. The authors thank F. Bélanger-Gariepy and M. Simard for X-ray crystallographic analysis, as well as Professor D. S. Bohle for initial help with X-ray analysis. We are grateful to NSERC and CIHR for a CHRP Grant. The Center for Self-Assembled Chemical Structures (CSACS) is acknowledged for financial support of crystallographic analyses. J.D.W. and F.R. acknowledge salary support and funding from the Canada Research Chairs program. F.R. is grateful to FQRNT for partial salary support. D.F.P. and F.R. acknowledge start-up funds from McGill University and INRS, respectively. D.F.P. (DuPont

Young Professor) and O.I. (DuPont Graduate Student) acknowledge support from DuPont USA. D.F.P. and F.R. are grateful to the AFOSR/IO and to the ACS PRF for partial support of this work.

Supporting Information Available: STM images of TMA–alcohol SAMNs obtained in various solvents, the details of the DFT calculations of the hydrogen-bonding energies, molecular models illustrating molecule–graphite interactions, calculations of the $\text{H}\cdots\text{H}$ distances for various tilt angles of the alcohols, NMR and mass spectra of the 1-undecyl monoester of TMA, cif files of the crystallographic analysis data of TMA•1-butanol, TMA•1-pentanol, and TMA•1-hexanol complexes and FFT of the dimerized alcohol. This material is available free of charge via the Internet at <http://pubs.acs.org>.

References and Notes

- Whitesides, G. M.; Grzybowski, B. *Science* **2002**, *295*, 2418.
- Rosei, F. *J. Phys.: Condens. Matter* **2004**, *16*, S1373.
- (a) Balzani, V.; Gómez-López, M.; Stoddart, J. F. *Acc. Chem. Res.* **1998**, *31*, 405. (b) Vickers, M. S.; Beer, P. D. *Chem. Soc. Rev.* **2007**, *36*, 211.
- (a) Bong, D. T.; Clark, T. D.; Granja, J. R.; Ghadiri, M. R. *Angew. Chem., Int. Ed.* **2001**, *40*, 988. (b) Shimizu, T.; Masuda, M.; Minamikawa, H. *Chem. Rev.* **2005**, *105*, 1401.
- Brunsveld, L.; Folmer, B. J. B.; Meijer, E. W.; Sijbesma, R. P. *Chem. Rev.* **2001**, *101*, 4071.
- DeVries, G. A.; Brunnbauer, M.; Hu, Y.; Jackson, A. M.; Long, B.; Neltner, B. T.; Uzun, O.; Wunsch, B. H.; Stellacci, F. *Science* **2007**, *315*, 358.
- Love, J. C.; Estroff, L. A.; Kriebel, J. K.; Nuzzo, R. G.; Whitesides, G. M. *Chem. Rev.* **2005**, *105*, 1103.
- Ulman, A. *Chem. Rev.* **1996**, *96*, 1533.
- Barth, J. V.; Costantini, G.; Kern, K. *Nature* **2005**, *437*, 671.
- Rabe, J. P.; Buchholz, S. *Science* **1991**, *253*, 424.
- (a) De Feyter, S.; De Schryver, F. C. *J. Phys. Chem. B* **2005**, *109*, 4290. (b) De Feyter, S.; De Schryver, F. C. *Chem. Soc. Rev.* **2003**, *32*, 139.
- (a) Stepanow, S.; Lingenfelder, M.; Dmitriev, A.; Spillmann, H.; Delvigne, E.; Lin, N.; Deng, X.; Cai, C.; Barth, J. V.; Kern, K. *Nat. Mater.* **2004**, *3*, 229. (b) Plass, K. E.; Kim, K.; Matzger, A. D. *J. Am. Chem. Soc.* **2004**, *126*, 9042. (c) Tao, F.; Bernasek, S. L. *J. Am. Chem. Soc.* **2005**, *127*, 12750.
- (a) Hipps, K. W.; Scudiero, L.; Barlow, D. E.; Cooke, M. P., Jr. *J. Am. Chem. Soc.* **2002**, *124*, 2126. (b) Otero, R.; Schöck, M.; Molina, L. M.; Lægsgaard, E.; Stensgaard, I.; Hammer, B.; Besenbacher, F. *Angew. Chem., Int. Ed.* **2005**, *44*, 2270.
- Lackinger, M.; Griessl, S.; Kampschulte, L.; Jamitzky, F.; Heckl, W. M. *Small* **2005**, *5*, 532.
- Lackinger, M.; Griessl, S.; Heckl, W. M.; Hietschold, M.; Flynn, G. W. *Langmuir* **2005**, *21*, 4984.
- Griessl, S.; Lackinger, M.; Edelwirth, M.; Hietschold, M.; Heckl, W. M. *Single Mol.* **2002**, *3*, 25.
- Surin, M.; Samori, P. *Small* **2007**, *3*, 190.
- Otero, R.; Naitoh, Y.; Rosei, F.; Jiang, P.; Thostrup, P.; Gourdon, A.; Lægsgaard, E.; Stensgaard, I.; Joachim, C.; Besenbacher, F. *Angew. Chem.* **2004**, *43*, 2092.
- Rosei, F.; Schunack, M.; Naitoh, Y.; Jiang, P.; Gourdon, A.; Lægsgaard, E.; Stensgaard, I.; Joachim, C.; Besenbacher, F. *Prog. Surf. Sci.* **2003**, *71*, 95.
- (20) Dickinson, R. G.; Raymond, A. L. *J. Am. Chem. Soc.* **1923**, *45*, 22. (b) The Cambridge Structural Database, version 5.27. <http://www.ccdc.cam.ac.uk> (last accessed October 2007). See also: Allen, F. H. *Acta Crystallogr.* **2002**, *B58*, 380.
- (a) Desiraju, G. R. *Crystal Engineering: The Design of Organic Solids*; Elsevier: Amsterdam, 1989. (b) Moulton, B.; Zaworotko, M. J. *Chem. Rev.* **2001**, *101*, 1629. (c) Wuest, J. D. *Chem. Commun.* **2005**, 5830.
- (a) Côté, A. P.; Benin, A. I.; Ockwig, N. W.; O'Keeffe, M.; Matzger, A. J.; Yaghi, O. M. *Science* **2005**, *310*, 1166. (b) Yip, H. L.; Ma, H.; Jen, A. K. Y.; Dong, J.; Parviz, B. A. *J. Am. Chem. Soc.* **2006**, *128*, 5672.
- Lee, A. Y.; Myerson, A. S. *MRS Bull.* **2006**, *31*, 875.
- Li, Z.; Han, B.; Wan, L. J.; Wandlowski, T. *Langmuir* **2005**, *21*, 6915.
- Sheerin, G.; Cafolla, A. A. *Surf. Sci.* **2005**, *577*, 211.
- Ye, Y.; Sun, W.; Wang, Y.; Shao, X.; Xu, X.; Cheng, F.; Li, J.; Wu, K. *J. Phys. Chem. C* **2007**, *111*, 10138.

- (27) Twofold packing of molecules with threefold symmetry on a substrate with threefold symmetry (HOPG) has been reported for conformationally mobile derivatives of triphenylene and hexabenzocoronene. However, such self-assembly does not have pronounced directionality: (a) Askadskaya, L.; Boeffel, C.; Rabe, J. P. *Ber. Bunsen-Ges. Phys. Chem. 1993*, *97*, 517. (b) Stabel, A.; Herwig, P.; Müllen, K.; Rabe, J. P. *Angew. Chem., Int. Ed.* **1995**, *34*, 1609.
- (28) Nath, K. G.; Ivasenko, O.; Miwa, J. A.; Dang, H.; Wuest, J. D.; Nanci, A.; Perepichka, D. F.; Rosei, F. *J. Am. Chem. Soc.* **2006**, *128*, 4212.
- (29) MacLeod, J. M.; Ivasenko, O.; Perepichka, D. F.; Rosei, F. *Nanotechnology* **2007**, *18*, 424031.
- (30) Dmitriev, A.; Lin, N.; Weckesser, J.; Barth, J. V.; Kern, K. *J. Phys. Chem. B* **2002**, *106*, 6907.
- (31) Ishikawa, Y.; Ohira, A.; Sakata, M.; Hirayama, C.; Kunitake, M. *Chem. Commun.* **2002**, 2652.
- (32) Su, G. J.; Zhang, H. M.; Wan, L. J.; Bai, C. L.; Wandlowski, Th. *J. Phys. Chem. B* **2004**, *108*, 1931.
- (33) Most recently, the third “superflower” polymorph, consisting of TMA molecules bound only by trimeric associations, has been observed as a stable structure on Au(111) under UHV conditions (ref 26) and also as a quasi-stable phase at solution–HOPG interface (ref 29).
- (34) Kitaigorodskii, A. I. *Acta Crystallogr.* **1965**, *18*, 585.
- (35) Duchamp, D. J.; March, R. E. *Acta Crystallogr.* **1969**, *B25*, 5.
- (36) The large calculated enthalpies of association arise from 10 individual hydrogen bonds present in these complexes.
- (37) Dale, S. H.; Elsegood, M. R. J.; Richards, S. J. *Chem. Commun.* **2004**, 1278.
- (38) (a) Segerman, E. *Acta Crystallogr.* **1965**, *19*, 789. (b) Kaneko, F. In *Crystallization Processes in Fats and Lipid Systems*; Garti, N., Sato, K., Eds.; Marcel Dekker: New York, 2001; pp 53–56.
- (39) However, high-resolution images of the inclined orientation with Θ close to 0° or 90° could also reveal two contrasting parallel lines of atoms with higher and lower profiles, corresponding to “high” and “low” hydrogen atoms.
- (40) McGonigal, G. C.; Bernhardt, R. H.; Thomson, D. J. *Appl. Phys. Lett.* **1990**, *57*, 28.
- (41) Liang, W.; Whangbo, M. H.; Wawkuszewski, A.; Cantow, H. J.; Magonov, S. N. *Adv. Mater.* **1993**, *5*, 817.
- (42) (a) Hibino, M.; Sumi, A.; Tsuchiya, H.; Hatta, I. *J. Phys. Chem. B* **1998**, *102*, 4544. (b) Wintgens, D.; Yablon, D. G.; Flynn, G. W. *J. Phys. Chem. B* **2003**, *107*, 173. (c) Wei, Y.; Kannappan, K.; Flynn, G. W.; Zimmit, M. B. *J. Am. Chem. Soc.* **2004**, *126*, 5318.
- (43) Between these two orientations, there is also a readjustment of the O(carbonyl)···H—O—C torsion angle, which engages one of the two lone pairs of the alcohol oxygen atom in hydrogen bonding with TMA.
- (44) Zhang, H. M.; Yan, J.-W.; Xie, Z.-X.; Mao, B.-W.; Xu, X. *Chem. Eur. J.* **2006**, *12*, 4006.
- (45) Lopinski, G. P.; Moffatt, D. J.; Wayner, D. D.; Wolkow, R. A. *Nature* **1998**, *392*, 909.
- (46) Lorenzo, M. O.; Baddeley, C. J.; Muryn, C.; Raval, R. *Nature* **2000**, *404*, 376.
- (47) Kühnle, A.; Lindertoh, T. R.; Hammer, B.; Besenbacher, F. *Nature* **2002**, *415*, 891.
- (48) Wei, Y.; Kannappan, K.; Flynn, G. W.; Zimmit, M. B. *J. Am. Chem. Soc.* **2004**, *126*, 5318.
- (49) (a) Eichhorst-Gerner, K.; Stabel, A.; Moessner, G.; Declercq, D.; Valiyaveetil, S.; Enkelmann, V.; Müllen, K.; Rabe, J. P. *Angew. Chem., Int. Ed.* **1996**, *35*, 1492. (b) Mena-Osteritz, E.; Bäuerle, P. *Adv. Mater.* **2001**, *13*, 243. (c) Grave, C.; Lentz, D.; Schäfer, A.; Samori, P.; Rabe, J. P.; Franke, P.; Schlüter, A. D. *J. Am. Chem. Soc.* **2003**, *125*, 6907. (d) Azumi, R.; Götz, G.; Debaerdemaeker, T.; Bäuerle, P. *Chem. Eur. J.* **2000**, *6*, 735.
- (50) (a) De Feyter, S.; Gesquière, A.; De Schryver, F.; Meiners, C.; Sieffert, M.; Müllen, K. *Langmuir* **2000**, *16*, 9887. (b) Kaneda, Y.; Stawasz, M. E.; Sampson, D. L.; Parkinson, B. A. *Langmuir* **2001**, *17*, 6185. (c) Stabel, A.; Heinz, R.; Rabe, J. P.; Wegner, G.; De Schryver, F. C.; Corens, D.; Dehaen, W.; Süling, C. *J. Phys. Chem.* **1995**, *99*, 8690.
- (51) (a) Hahn, T.; Janovec, V.; Klapper, H. *Ferroelectrics* **1999**, *222*, 11. (b) Hahn, T.; Klapper, H. *International Tables for Crystallography*; Authier, A., Ed.; Kluwer Academic Publishers: 2003; Volume D, Section 3.3.
- (52) If the alkyl chains in reflectional domains are oriented along different “zigzag” axes of graphite, then the angle between TMA tapes will be $2\alpha-60$.
- (53) Kim, K.; Plass, K. E.; Matzger, A. J. *J. Am. Chem. Soc.* **2005**, *127*, 4879.
- (54) Plass, K. E.; Matzger, A. *Chem. Comm.* **2006**, 3486.
- (55) Horcas, I.; Fernandez, R.; Gomez-Rodriguez, J. M.; Colchero, J.; Gomez-Herrero, J.; Baro, A. M. *Rev. Sci. Instrum.* **2007**, *78*, 013705.
- (56) Frisch, M. J.; Trucks, G. W.; Schlegel, H. B.; Scuseria, G. E.; Robb, M. A.; Cheeseman, J. R.; Montgomery, J. A., Jr.; Vreven, T.; Kudin, K. N.; Burant, J. C.; Millam, J. M.; Iyengar, S. S.; Tomasi, J.; Barone, V.; Mennucci, B.; Cossi, M.; Scalmani, G.; Rega, N.; Petersson, G. A.; Nakatsuji, H.; Hada, M.; Ehara, M.; Toyota, K.; Fukuda, R.; Hasegawa, J.; Ishida, M.; Nakajima, T.; Honda, Y.; Kitao, O.; Nakai, H.; Klene, M.; Li, X.; Knox, J. E.; Hratchian, H. P.; Cross, J. B.; Bakken, V.; Adamo, C.; Jaramillo, J.; Gomperts, R.; Stratmann, R. E.; Yazyev, O.; Austin, A. J.; Cammi, R.; Pomelli, C.; Ochterski, J. W.; Ayala, P. Y.; Morokuma, K.; Voth, G. A.; Salvador, P.; Dannenberg, J. J.; Zakrzewski, V. G.; Dapprich, S.; Daniels, A. D.; Strain, M. C.; Farkas, O.; Malick, D. K.; Rabuck, A. D.; Raghavachari, K.; Foresman, J. B.; Ortiz, J. V.; Cui, Q.; Baboul, A. G.; Clifford, S.; Cioslowski, J.; Stefanov, B. B.; Liu, G.; Liashenko, A.; Piskorz, P.; Komaromi, I.; Martin, R. L.; Fox, D. J.; Keith, T.; Al-Laham, M. A.; Peng, C. Y.; Nanayakkara, A.; Challacombe, M.; Gill, P. M. W.; Johnson, B.; Chen, W.; Wong, M. W.; Gonzalez, C.; Pople, J. A. *Gaussian 03*, revision D.01; Gaussian, Inc.: Wallingford, CT, 2004.